Microchimica Acta (2024) 191:715
https://doi.org/10.1007/s00604-024-06723-4

RESEARCH

Nanoplasmonic microarray–based solid-phase amplification for highly sensitive and multiplexed molecular diagnostics: application for detecting SARS-CoV-2

Ji Young Lee[1] · Hyowon Jang[2] · Sunjoo Kim[3] · Taejoon Kang[2,4] · Sung-Gyu Park[1] · Min-Young Lee[1]

Received: 29 July 2024 / Accepted: 21 September 2024 / Published online: 29 October 2024
© The Author(s) 2024

Abstract

A novel approach is introduced using nanoplasmonic microarray–based solid-phase recombinase polymerase amplification (RPA) that offers high sensitivity and multiplexing capabilities for gene detection. Nanoplasmonic microarrays were developed through one-step immobilization of streptavidin/biotin primers and fine-tuning the amplicon size to achieve high plasmon-enhanced fluorescence (PEF) on the nanoplasmonic substrate, thereby improving sensitivity. The specificity and sensitivity of solid-phase RPA on nanoplasmonic microarrays was evaluated in detecting E, N, and RdRP genes of SARS-CoV-2. High specificity was achieved by minimizing primer-dimer formation and employing a stringent washing process and high sensitivity obtained with a limit of detection of four copies per reaction within 30 min. In clinical testing with nasopharyngeal swab samples ($n = 30$), the nanoplasmonic microarrays demonstrated a 100% consistency with the PCR results for detecting SARS-CoV-2, including differentiation of Omicron mutations BA.1 and BA.2. This approach overcomes the sensitivity issue of solid-phase amplification, as well as offers rapidity, high multiplexing capabilities, and simplified equipment by using isothermal reaction, making it a valuable tool for on-site molecular diagnostics.

Keywords Nanoplasmonic microarrays · Multiplex molecular diagnostics · Solid-phase amplification · SARS-CoV-2 · Differentiation of mutations

With the increasing risk of infectious outbreaks and the emergence of diverse infection factors and variants, there is a pressing need for highly sensitive and multiplex on-site gene detection technology. This technology enables the rapid identification of multiple infectious agents and their variations, facilitating quick response and appropriate treatment, thereby reducing antibiotic resistance and effective outbreak management. However, conventional real-time PCR is typically limited to multiplexing 2–5 targets in a single test due to the overlapping fluorescence spectra of dyes [1]. Over the past decade, several multiplex panels, such as Luminex xTAG and BioFire FilmArray, have gained FDA approval for clinical diagnostics [2]. Luminex xTAG technology relies on fluorescent-barcoded paramagnetic beads and the principles of flow cytometry [3, 4], enabling the simultaneous detection of over 100 different target genes in a single test. In contrast, BioFire FilmArray employs melting curve analysis [5, 6] to simultaneously detect over 40 different target genes in a single test. Despite their capability to perform highly

✉ Sung-Gyu Park
sgpark@kims.re.kr

✉ Min-Young Lee
myay0615@kims.re.kr

1 Advanced Bio and Healthcare Materials Research Division, Korea Institute of Materials Science (KIMS), 797, Changwon-Daero, Seongsan-Gu, Changwon-Si, Gyeongsangnam-Do 51508, Republic of Korea

2 Bionanotechnology Research Center, Korea Research Institute of Bioscience and Biotechnology (KRIBB), 125, Gwahak-Ro, Yuseong-Gu, Daejeon 34141, Republic of Korea

3 Department of Laboratory Medicine, Gyeongsang National University College of Medicine, 79 Gangnam-Ro, Jinju, Gyeongsangnam-Do 52727, Republic of Korea

4 School of Pharmacy, Sungkyunkwan University, 2066, Seobu-Ro, Jangan-Gu, Suwon, Gyeonggi-Do 16419, Republic of Korea

multiplexed PCR assays, these technologies have limitations, such as the need for expensive platforms and lower sensitivity compared to real-time PCR [7, 8], which limits their widespread adoption. DNA microarrays enable highly multiplexed detection using a single fluorescence dye and a laser [9, 10]. However, these platforms require additional DNA denaturation and hybridization processes, which can result in cross-hybridization and reduced specificity. This additional step also extends the testing time to 1- to 42-h post-amplification [11–13].

In contrast, solid-phase nucleic acid amplification presents a promising approach for achieving high levels of multiplexing through position-based detection of amplified DNA immobilized on a solid-state support [14, 15]. Solid-phase amplification offers advantages in multiplex detection, such as eliminating additional hybridization processes and achieving high specificity in highly multiplexed reactions by localizing them to a solid surface and reducing non-specific amplification. Furthermore, it simplifies equipment by using a single laser. However, solid-phase amplification faces challenges related to lower amplification efficiency due to non-free primers and environmental steric hindrance, resulting in reduced sensitivity compared to DNA microarray hybridization [16]. On the other hand, the high temperature of around 90 °C used in solid-phase PCR can damage surface layers used for primer immobilization, especially self-assembled monolayers, leading to poor reproducibility [17]. Recent strategies for solid-phase isothermal recombinase polymerase amplification (RPA) have aimed to enhance sensitivity and reproducibility. Absorbance detection using biotinylated dNTPs and streptavidin-polyhorseradish peroxidase achieved a limit of detection (LOD) of 363 fM [18]. Electrochemical detection using ferrocene-labeled dNTPs achieved LOD of 13 fM (approximately 10^5 copies DNA/reaction) [19]. Another electrochemical detection approach using microfabricated ITO electrodes, along with three primers (surface-bound forward primer, solution reverse primer, and extremely low concentration of solution forward primer), achieved LOD of 0.1 fM (approximately 10^3 copies DNA/reaction) [17]. Additionally, LED flashlight visual detection of solid-phase RPA coupled with CRISPR reported LOD of 20 copies/μL (approximately 10^3 copies/reaction) [20].

In this study, we present nanoplasmonic microarray–based solid-phase multiplex RPA for highly sensitive and highly multiplex molecular detection. In our previous report, we have reported the plasmonic isothermal RPA array chip [21]. However, to facilitate practical clinical applications, it was necessary to improve sensitivity and devise a new spotting strategy for the fabrication of miniaturized microarray chips. To enhance sensitivity, we optimized amplicon lengths to maximize plasmonic-enhanced fluorescence (PEF) on the nanoplasmonic substrate. Furthermore, the nanoplasmonic microarray was fabricated through one-step spotting of mixtures of streptavidin and excess biotin-labeled forward primer. We assessed specificity and sensitivity of the solid-phase multiplex RPA on the nanoplasmonic microarray for detecting E, N, and RdRP genes of SARS-CoV-2. Clinical performance was assessed using nasopharyngeal swab samples collected from individuals who tested positive for either the SARS-CoV-2 wild type or the Omicron variants (BA.1 and BA.2), as well as from negative samples.

Materials and methods

SARS-CoV-2 RNA extracted from viral cell culture

SARS-CoV-2 RNAs extracted from viral cell cultures, including wild type (NCCP 43346), Omicron variants BA.1 (NCCP 43408) and BA.2 (NCCP 43412), were obtained from the National Culture Collection for Pathogens of Korea Disease Control and Prevention Agency (KCDC) (Cheongju, South Korea).

Primer design and synthesis

Oligonucleotide primers targeting E, N, and RdRP genes, as well as Omicron variants BA.1 and BA.2, were synthesized (Bioneer, Daejeon, South Korea). The forward primers, intended for immobilization on the nanoplasmonic surface, were biotinylated, and the reverse primers were labeled with cyanine 5 (Cy5). Table 1 displays the primer sequences.

cDNA synthesis

Complementary DNA (cDNA) was synthesized using a reverse transcription kit (Thermo Fisher, Carlsbad, CA, USA) and random primers (Thermo Fisher, Carlsbad, CA, USA) following the manufacturer's recommendations. In brief, 2 μL of total RNA was added to mixture containing 10 × RT buffer, 0.8 μL of 25 × dNTP mix, 2 μL of 10 × random primers, 1.0 μL of MultiScribe Reverse Transcriptase, and 3.2 μL of nuclease-free water. Subsequently, cDNA synthesis was carried out at 25 °C for 10 min, 37 °C for 120 min, and 85 °C for 5 min. The synthesized cDNA was then stored at − 70 °C until further use. This step can be eliminated by directly adding reverse transcriptase to the RPA reaction.

Fabrication of 3D nanoplasmonic substrate

PET film was subjected to Ar plasma treatment for 2 min using customized RF ion-etching instrument (LAT, South Korea) with the following fixed parameters: 5 sccm Ar flow, 80 mTorr pressure, and plasma power of

Table 1 Primer sequences

Target gene	Primer sequence 5'-3'	Amplicon size (bp)
E	Forward: [Biotin] TTTTTTTTTTGAAGAGACAGGTACGTTAATAGTTAATAGCGTA Reverse: [Cy5] AAAAAGAAGGTTTTACAAGACTCACGTTAACsA	151
N	Forward: [Biotin]TTTTTTTTTTCGGTGATGCTGCTCTTGCTTTGCTGCTGCTTG Reverse: [Cy5] AGTGACAGTTTGGCCTTGTTGTTGTTGGCCTT	100
	Forward: [Biotin] TTTTTTTTTTACTCCAGGCAGCAGTAGGGGAACTTCTCCTGC Reverse: [Cy5] AGTGACAGTTTGGCCTTGTTGTTGTTGGCCTT	150
	Forward: [Biotin]TTTTTTTTTTCCTCTTCTCGTTCCTCATCACGTAGTCGCAAC Reverse: [Cy5] AGTGACAGTTTGGCCTTGTTGTTGTTGGCCTT	197
RdRP	Forward: [Biotin] TTTTTTTTTTTATGCCATTAGTGCAAAGAATAGAGCTCGCAC Reverse: [Cy5] CAACCACCATAGAATTTGCTTGTTCCAATTAC	158
Omicron variant BA.1	Forward: [Biotin] TTTTTTTTTTTATGTTACTTGGTTCCATGTTAT Reverse: [Cy5] ACTTCTCAATGGAAGCAAAATAAACA	110
Omicron variant BA.2	Forward: [Biotin] TTTTTTTTTTTTGTTAATCTTATAACCAGAACTCAAT Reverse: [Cy5] AGAACAAGTCCTGAGTTGAATGTA	113

100 W. A 100-nm-thick Au layer was then deposited on PET nanopillars at a rate of 2.0 Å s^{-1} under base pressure of 9.6×10^{-6} Torr using thermal evaporation system (LAT, South Korea). Subsequently, 1H,1H,2H,2H-perfluorodecanethiol (PFDT) was applied, followed by thermal evaporation of Au onto PFDT-treated Au/PET nanopillar substrate at 0.3 Å s^{-1}. The 3D plasmonic substrate was cut into 9 mm × 9 mm pieces to fabricate the microarray chip.

Comparison of fluorescence signals of RPA products on the nanoplasmonic substrate according to amplicon size

The nanoplasmonic substrate was cut into 5 mm × 5 mm pieces. These substrate pieces were soaked in a solution of streptavidin (100 µL, 1.8 µM in PBS) and incubated in a refrigerator at 4 °C overnight. Following this, substrates underwent three washes with nuclease-free water and one wash with phosphate buffered saline (PBS pH 7.4) containing 0.05% Tween 20.

To assess the impact of amplicon length on PEF, conventional liquid-phase PCR amplification products were synthesized. Primer sequences were detailed in Table 1. The biotin-labeled forward primers and Cy5-labeled reverse primers were designed to target N gene and produce PCR products (double-stranded DNA) of final sizes of 100 bp, 150 bp, and 197 bp. Primers were used at a concentration of 500 nM, and cDNA synthesized from the SARS-CoV-2 RNA gene, serving as the target gene, was used at a concentration of 4×10^4 copies/reaction. For complete PCR reaction, 40 cycles were run using AccuPower® PCR PreMix (Bioneer, Daejeon, South Korea) according to the manufacturer's protocol. The resulting PCR products were applied to streptavidin pre-coated nanoplasmonic substrates and washed three times with DEPC-treated water.

Preparation of nanoplasmonic microarrays

Streptavidin and each biotin-modified forward primer were mixed in DEPC-treated water, resulting in final concentrations of 100 nM and 2.5 µM, respectively. The mixture was then spotted onto the nanoplasmonic substrate (9 mm × 9 mm) at fixed volumes of 20 nL, 50 nL, or 100 nL using an OptiSpotTM Microarrayer (ebiogen Inc., Seoul, South Korea). The distance between individual spots was set at 2 mm. The spotted nanoplasmonic substrate was incubated in a refrigerator at 4 °C overnight for immobilization. Subsequently, the nanoplasmonic substrate was washed three times with DEPC-treated water to remove excess streptavidin and oligonucleotides. It was then incubated in a 0.5% BSA solution at 25 °C for 2 h to block the non-spotted areas. Afterward, the nanoplasmonic substrate was washed three times with DEPC-treated water and slowly dried at room temperature.

Solid-phase RPA on the nanoplasmonic microarrays

The nanoplasmonic microarray was affixed to a glass slide, and PDMS frame was attached to contain the RPA reaction solution. Then, solid-phase RPA reaction was performed using TwistAmp® Liquid Basic (TwistDX, Cambridge, UK) following the manufacturer's protocol with slight modifications. To prepare the RPA reaction solution, each reverse primer (10 µM) was added at 2.5 µL (with the forward primer excluded) to a 0.2-mL PCR tube, along with 29.5 µL of primer-free rehydration buffer. The template and water were then added to bring the volume up to 47.5 µL. Finally,

2.5 µL of 280 mM magnesium acetate (MgOAc) was added and mixed thoroughly. A total of 50 µL of the RPA reaction solution was loaded onto the nanoplasmonic microarray. RPA reaction was conducted at constant temperature of 39 °C using ThermoMixer C (Eppendorf, Hamburg, Germany) for 30 min. After the reaction, the nanoplasmonic microarrays were washed three times with DEPC-treated water.

Fluorescence detection

Fluorescence images were acquired using an InnoScan 710 Microarray Scanner with laser excitation wavelength of 635 nm (Innopsys, Carbonne, France). Subsequent analysis of fluorescence intensities was performed using the scanner's software.

Clinical sample test

Clinical samples were obtained from Gyeongsang National University College of Medicine, Jinju, South Korea, with approval from the Institutional Review Board (IRB approval number: 2022–10-012). Nasopharyngeal swabs were collected from a total of 20 patients, including those infected with SARS-CoV-2 wild-type ($n=10$), Omicron variant BA.1 ($n=5$), Omicron variant BA.2 ($n=5$), and negative controls ($n=10$) as determined by PCR. The swabs were placed in virus transport media (UTM, Copan Diagnostics Inc., Murrieta, CA, USA). All collected samples were promptly stored at − 85 °C until further analysis. Viral RNA was extracted from the clinical samples using QIAmp Viral RNA Mini Kit (Qiagen, Germany), following the manufacturer's protocol. Subsequently, cDNA synthesis was performed. Nanoplasmonic microarrays were fabricated by applying primers designed to target E, N, RdRP, Omicron variant BA.1, and Omicron variant BA.2. A spotting volume of 50 nL was used for this process, following the same protocol as described above. Solid-phase RPA was then performed on the nanoplasmonic microarray. The RPA reaction solution included reverse primers designed to target E, N, RdRP, Omicron variant BA.1, and Omicron variant BA.2, each at a concentration of 500 nM. The amplification process followed the same protocol as described above.

Results and discussions

Fabrication strategy of nanoplasmonic microarrays

Figure 1 illustrates flow diagram for preparation of nanoplasmonic microarray and assay protocol capable of solid-phase isothermal amplification, simultaneously detecting various target genes. In this study, we employed the nanoplasmonic substrate based on our previous work, featuring a 3D structure of densely decorated Au nanopillars with AuNPs (as shown in SEM images inserted in Fig. 1A and Figure S1) [21]. Solid-phase amplification presents greater challenges compared to hybridization-based microarrays. This is because solid-phase amplification necessitates the direct interaction of the target gene, which, in the case of SARS-CoV-2, has a genome size ranging from 29.8 to 29.9 kb, with immobilized primers. In contrast, hybridization-based microarrays rely on the interaction of amplified products, typically ranging from approximately 200 to 500 bp in size, with fixed probes. Therefore, for solid-phase amplification, optimizing primer density is crucial to facilitate effective binding to target gene and enhance overall amplification process [22]. Chemical immobilization does not afford direct control over the spacing between primers. Consequently, achieving precise control and optimization of primer spacing demands substantial experimental effort. To address this, we utilized the streptavidin/biotin-labeled primer to adjust the spacing between immobilized primers to be approximately over 5 nm, based on calculations corresponding to the size of streptavidin–biotin structure. In previous approaches utilizing streptavidin–biotin interactions, biotin-labeled probes are typically immobilized after pre-coating surface with streptavidin [23–26]. However, when applying an aqueous solution of biotin-labeled forward primer onto a hydrophilic substrate pre-coated with streptavidin, the solution tends to spread, leading to overlapping or merging of adjacent spots, which requires increased spacing to prevent cross-contamination or signal interference. This ultimately leads to larger microarrays. To overcome this, we adopted one-step approach by directly spotting mixtures of streptavidin and excess biotin-labeled forward primer on the hydrophobic nanoplasmonic substrate, as shown in Fig. 1. The streptavidin–biotin interaction is one of the strongest non-covalent bonds known in biological systems, characterized by an extraordinarily low dissociation constant (Kd) around 10^{-15} M. This interaction is remarkably stable and nearly irreversible under most conditions [27]. This stability allows pre-bound streptavidin/biotin-labeled primers to maintain their structure after binding to gold surface. This approach maintains droplet shape with a low contact angle, enabling immobilization of the forward primer in a confined area and narrowing the spot spacing.

Subsequently, we applied bovine serum albumin (BSA) to coat the uncoated surface of the spotted nanoplasmonic substrate. It is crucial to optimize BSA concentration to ensure thorough coverage of the uncoated surface while preventing unintentional detachment of streptavidin/biotin-primer and avoiding interference with the interaction between target gene and fixed primers. We determined the optimal BSA concentration to be 0.5% by comparing fluorescence signals after solid-phase amplification step, as shown in Fig. 2A.

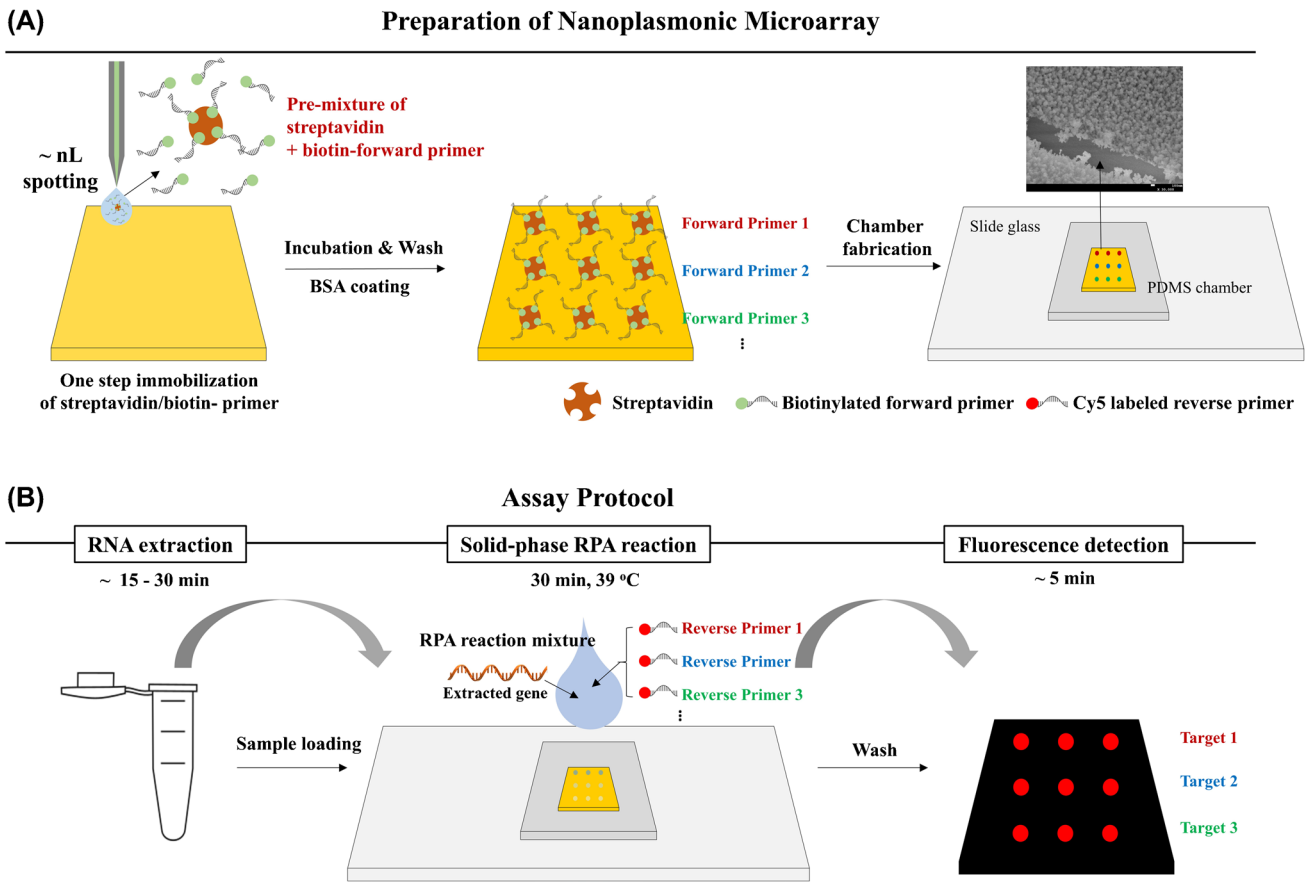

Fig. 1 Schematic illustration of **A** preparation of nanoplasmonic microarray and **B** assay protocol for solid-phase multiplex RPA

Optimization of amplicon size for high PEF effect

The distance between fluorophore and surface of nanoplasmonic substrate is critical for achieving highly efficient PEF effect. Therefore, prior to preparing the nanoplasmonic microarray, we assessed PEF effects in relation to amplicon size. Following the recommendations from the RPA kit manufacturer (TwistDx), there may not be a strict lower limit for the size of RPA amplicons. However, it is generally advised that RPA amplicons should be longer than approximately 80 base pairs, with ideal size ranging from 100 to 200 base pairs for rapid kinetics. Therefore, we designed biotin-labeled forward primers and Cy5-labeled reverse primers targeting N gene of SARS-CoV-2 to achieve amplicon sizes of 100 bp, 150 bp, and 197 bp corresponding to lengths of 34 nm, 51 nm, and 68 nm, respectively, when fully extended, as detailed in Table 1. The primers and products (double stranded DNA) employed in PCR and RPA can be identical. To ensure amplification of all primers, conventional liquid-phase PCR using each biotin-labeled forward primer and Cy5-labeled reverse primer was conducted for 40 cycles. The PCR product was then bound to streptavidin pre-coated nanoplasmonic substrate. As shown in Fig. 2B, smaller amplicon sizes were correlated with higher fluorescence signals. This outcome can be attributed to increased PEF efficiency resulting from decreased distance between fluorophore and surface of nanoplasmonic substrate, a well-known phenomenon [28]. Furthermore, DNA fragments exhibit different behaviors depending on their length relative to persistence length, approximately 50 nm [29, 30]. For DNA fragments shorter than 50 nm, the molecule tends to behave as a rigid rod, maintaining a straight and upright orientation due to stiffness. The lack of significant interaction with surface allows these shorter fragments to remain relatively elevated and resist bending, even in dry state during our detection process. On the other hand, DNA fragments longer than 50 nm, while still semi-rigid, begin to show increased flexibility. Even with minimal surface interaction, these longer fragments are more likely to bend or partially lie down due to greater susceptibility to bending forces in dry state, which can result in quenching of fluorescence. Therefore, in PEF-based surface assays, optimized shorter fragments are preferable to avoid quenching and enhance PEF effect.

Next, we assessed sensitivity of solid-phase RPA on the nanoplasmonic substrate. As demonstrated in Fig. 2C, amplicon sizes of 100 bp and 150 bp allowed detection of

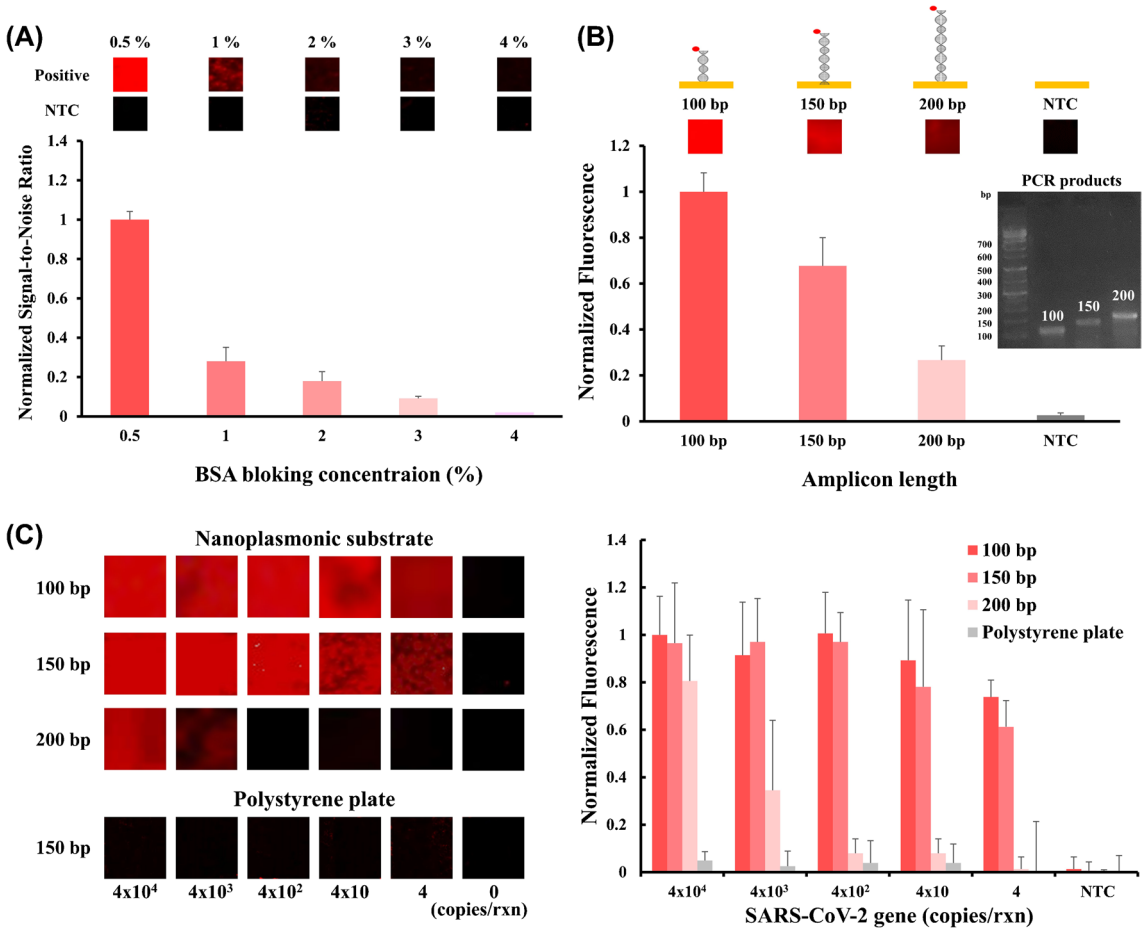

Fig. 2 Optimization of BSA blocking and amplicon length. **A** Normalized signal-to-noise ratios according to BSA blocking concentration. **B** Comparison of fluorescence signals of liquid-phase PCR products on the nanoplasmonic substrate according to their amplicon length and gel electrophoresis of the liquid-phase PCR products (inserted image). **C** Comparison of fluorescence signals of solid-phase RPA on the nanoplasmonic substrate according to their amplicon length and on a polystyrene plate (NTC; negative control)

target gene concentrations as low as 4 copies/reaction, while 200 bp amplicon could detect down to 4×10^3 copies/reaction. These results may be influenced by steric hindrance effects and duration of amplification along amplicon length, as well as reduced PEF efficiency resulting from increased distance between fluorophore and surface of nanoplasmonic substrate. Consequently, we confirmed that adjusting amplicon size enhances the high sensitivity of nanoplasmonic substrate for solid-phase RPA. Accordingly, we determined that an amplicon length of 100–150 bp is optimal for achieving sensitive detection.

Following this, we conducted comparison between fluorescence signals obtained from solid-phase RPA on nanoplasmonic substrate and those on crystal-grade polystyrene plate, common material used in enzyme-linked immunosorbent assays (ELISA). The surface of crystal-grade polystyrene plate was coated using the same method described above, and solid-phase RPA was performed with primers designed to amplify an amplicon size of 150 bp. As shown in Fig. 2C, the polystyrene plate displayed no distinguishable fluorescence signal even when up to 4×10^4 copies/reaction of target gene were used under the same conditions. We confirmed that the nanoplasmonic substrate exhibits exceptionally high sensitivity for detecting solid-phase DNA amplicons. This phenomenon is attributable to the increased volume-to-surface ratio provided by its three-dimensional architecture as well as the PEF effect. This structural feature augments number of available binding sites, enhancing capture efficiency of fluorescent probes, and reduces steric hindrance between target gene and immobilized primers, thereby improving kinetics of solid-phase amplification.

Specificity and sensitivity of nanoplasmonic microarrays for SARS-CoV-2

The specificity and sensitivity of the nanoplasmonic solid-phase RPA microarrays were assessed using SARS-CoV-2 gene. Detecting multiple targets of SARS-CoV-2 is valuable

for enhancing accuracy, reliability, and efficiency of COVID-19 testing, while also providing critical insights into virus's genetic diversity and mutations. We designed primers for wild-type E, N, and RdRP genes of SARS-CoV-2 to generate amplicons of approximately 150 bp, considering sensitivity and potential cross-reactions during multiplexing.

For specificity test, forward primers targeting E, N, and RdRP genes of SARS-CoV-2 were immobilized in 3×3 spots at 50 nL spotting volume. Solid-phase single-plex RPA on nanoplasmonic microarrays, using one reverse primer targeting E, N, or RdRP gene and 4×10^4 copies/reaction of SARS-CoV-2 gene, revealed that fluorescence signals were detected only at spots where target primers were immobilized for E, N, or RdRP genes, as shown in Fig. 3A. The high specificity of solid-phase amplification can be achieved through a combination of factors, including fixed primers minimizing primer-dimer formation, spatial confinement, steric hindrance, and the implementation of stringent washing steps. Moreover, in fluorescence-based detection, to evaluate false positive signals, negative control is typically

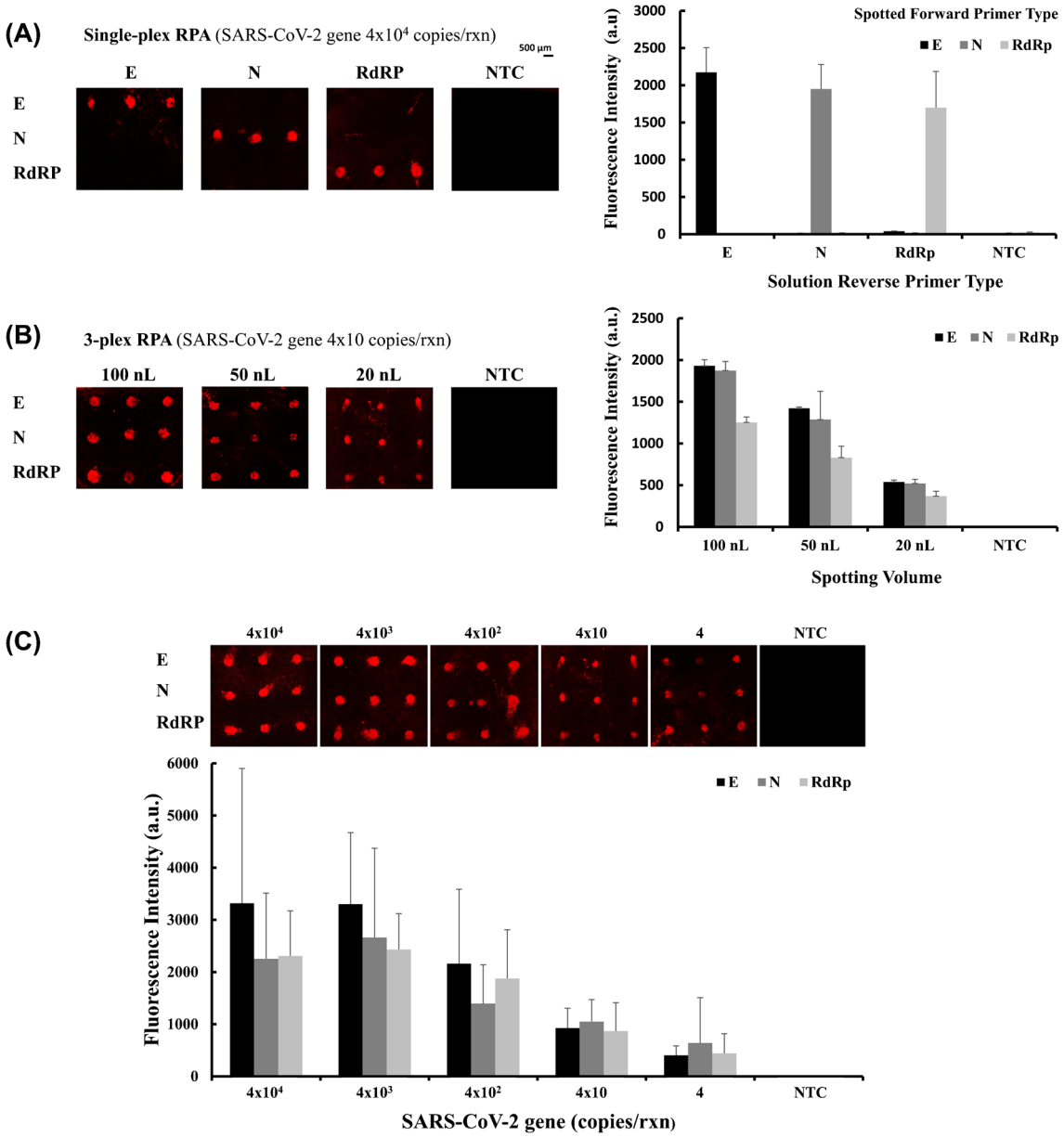

Fig. 3 Specificity and sensitivity tests. **A** Specificity test of solid-phase single-plex RPA on the nanoplasmonic microarray immobilized with forward primers targeting the E, N, and RdRP gene. **B** Comparison of fluorescence signals of solid-phase 3-plex RPA on the nanoplasmonic microarray based on the spotting volume of the forward primer. **C** Sensitivity test of solid-phase 3-plex RPA on the nanoplasmonic microarray at a spotting volume of 20 nL

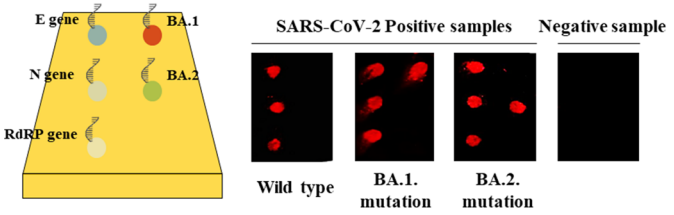

Samples	SARS-CoV-2 Positive (n=20)			SARS-CoV-2 Negative samples (n=10)
	Wild type (n=10)	BA.1. mutation (n=5)	BA.2. mutation (n=5)	
SARS-CoV-2 Wild type	10	0	0	0
BA.1. mutation	0	5	0	0
BA.2. mutation	0	0	5	0
Negative	0	0	0	10
Consistency	100 %	100 %	100 %	100 %

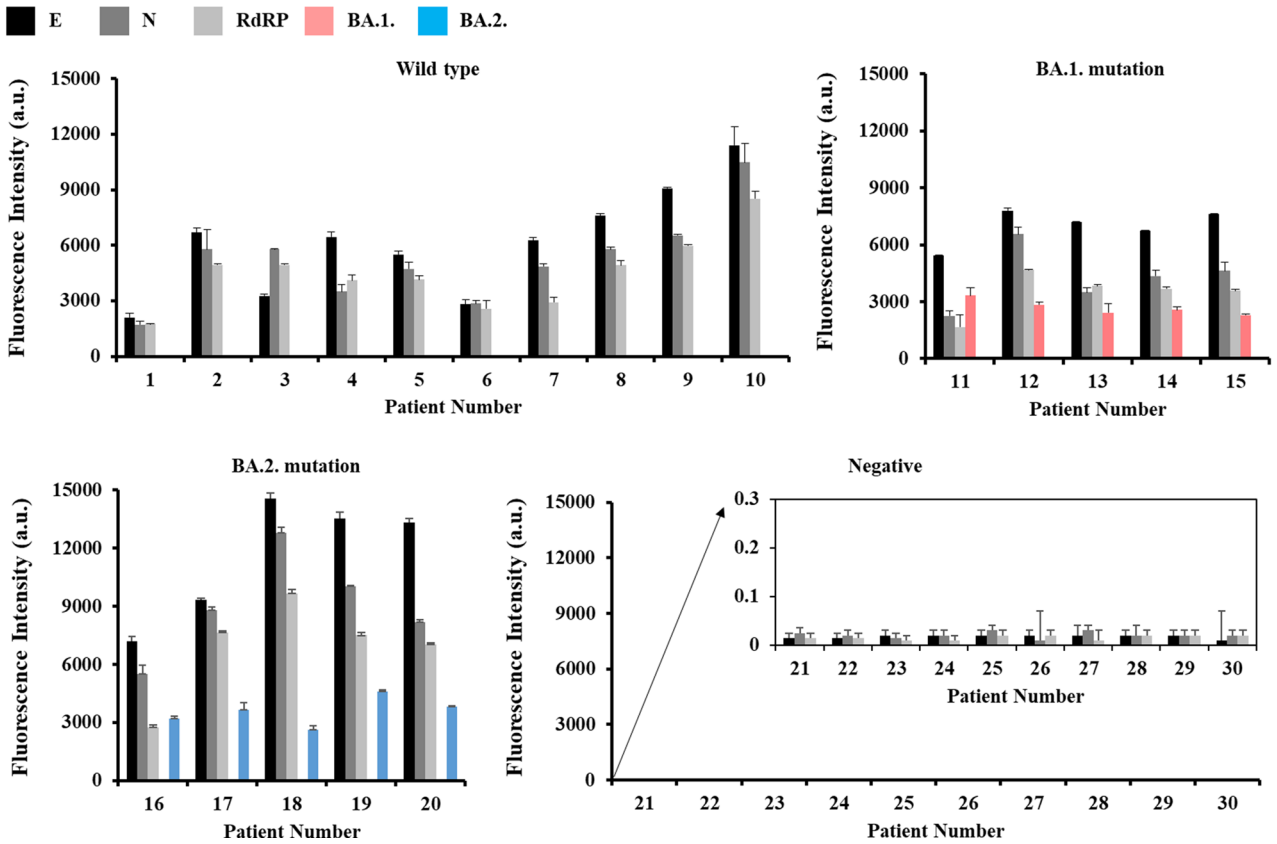

Fig. 4 Clinical sample test. Solid-phase 5-plex RPA on the nanoplasmonic microarray, immobilized with forward primers targeting the E, N, and RdRP genes for SARS-CoV-2 wild-type and Omicron variants BA.1 and BA.2, using clinical nasopharyngeal swab samples confirmed by PCR, as detailed in Table 2

included on the same chip. However, the microarray-based approach allows for intuitive observation of signals relative to background without need for negative control on the chip.

Then, we assessed sensitivity based on spotting volume of streptavidin/biotin-forward primer solution. We immobilized forward primers targeting E, N, and RdRP genes of SARS-CoV-2 in 3 × 3 spots at spotting volumes of 100 nL, 50 nL, and 20 nL. As shown in Fig. 3B, 3-plex solid-phase RPA on the nanoplasmonic microarrays exhibited higher fluorescence intensities with increasing spotting volume. All genes were detectable at 4 × 10 copies/reaction of the SARS-CoV-2 gene for all spotting volumes, even at the smallest 20 nL spotting volume. Subsequently, we evaluated fluorescence intensities of 3-plex solid-phase nanoplasmonic microarray with 20 nL spotting volume, using SARS-CoV-2 gene concentrations ranging from 4 copies/reaction to 4×10^4 copies/reaction. The fluorescence signals tended to increase as SARS-CoV-2 gene concentration increased. In the 30-min RPA reaction, the fluorescence signals saturated at 4×10^3 copies/reaction. Even at 4 copies/reaction, the fluorescence signals of all genes (E, N, and RdRP) were clearly distinguishable from the negative control. The high sensitivity is believed to be attributed to the optimized PEF effect of the

Table 2 The PCR Ct values of the clinical nasopharyngeal swab samples: (A) Positive SARS-CoV-2 wild type samples with Ct values of 28.1–34.2 for N gene. (B) Positive SARS-CoV-2 Omicron mutation BA.1 samples with Ct values of 15.95–36.70 for N gene. (C) Positive SARS-CoV-2 Omicron mutation BA.2 samples with Ct values of 13.04–25.37 for N gene. (D) Negative samples

A. Positive SARS-CoV-2 wild type			
Number	**PCR Ct value**		
	ORF	**N**	**S**
1	33.2	**34.2**	31.1
2	33.2	30.22	28.84
3	32.2	31.2	27.07
4	30.2	29.4	28.3
5	28.73	33.1	29.27
6	29.95	29.16	28.73
7	26.3	25.4	25.2
8	25.2	28.3	25.1
9	25.2	29.1	24.3
10	24.88	**28.1**	23.07
B. Positive SARS-CoV-2 Omicron mutation BA.1			
Number	**PCR Ct value**		
	ORF	**N**	
11	34.90	**36.70**	
12	24.77	25.47	
13	23.16	24.65	
14	16.68	17.97	
15	14.59	**15.95**	
C. Positive SARS-CoV-2 Omicron mutation BA.2			
Number	**PCR Ct value**		
	ORF	**N**	
16	25.96	**25.37**	
17	19.24	18.45	
18	19.20	18.62	
19	15.31	14.50	
20	13.33	**13.04**	
D. Negative			
Number	**PCR Ct value**		
	ORF	**N**	**S**
21	N/A	N/A	N/A
22	N/A	N/A	N/A
23	N/A	N/A	N/A
24	N/A	N/A	N/A
25	N/A	N/A	N/A
26	N/A	N/A	N/A
27	N/A	N/A	N/A
28	N/A	N/A	N/A
29	N/A	N/A	N/A
30	N/A	N/A	N/A

nanoplasmonic substrate, achieved by adjusting the amplicon size to approximately 150 bp.

Evaluation of nanoplasmonic microarrays using clinical swab samples

To preliminarily evaluate SARS-CoV-2 detection in clinical settings, we prepared a 5-plex nanoplasmonic microarray by spotting five forward primers for wild-type E, N, and RdRP genes, along with mutant variants of Omicron BA.1 and Omicron BA.2, using spotting volume of 100 nL. The primers for E, N, and RdRP genes were designed to have an amplicon size of 150 bp. In contrast, the primers for mutant genes of Omicron BA.1 and BA.2 were specifically designed to produce an amplicon size of approximately 110 bp to enhance the PEF effect (Table 1). This strategic choice considered the possibility of mutant-type genes being present in smaller quantities compared to their wild-types.

We evaluated the 5-plex nanoplasmonic microarray using clinical nasopharyngeal swab samples, which were positive for SARS-CoV-2 wild type ($n = 10$), Omicron BA.1 ($n = 5$), Omicron BA.2 ($n = 5$), or negative controls ($n = 10$) as determined by PCR. The Ct values obtained from PCR for each gene have been listed in Table 2. The SARS-CoV-2 wild type exhibited Ct values for the N gene ranging from 28.1 to 34.2. In the case of BA.1 mutation, the Ct values for N gene ranged between 15.95 and 36.70, while for BA.2 mutation, the Ct values ranged between 13.04 and 25.37. As shown in Fig. 4, the nanoplasmonic microarray exhibited a 100% consistency rate with the PCR results across all samples. Specifically, SARS-CoV-2 wild-type samples exhibited fluorescence signals at E, N, and RdRP gene spots and no fluorescence signal at Omicron BA.1 and BA.2 spots. In contrast, Omicron BA.1 samples showed strong fluorescence signals at BA.1 gene spots, as well as at E, N, and RdRP spots. Similarly, Omicron BA.2 samples displayed strong fluorescence signals at BA.2 gene spot, as well as at E, N, and RdRP spots. All negative samples exhibited no detectable fluorescence signals at any spots. As a result, we have verified that the solid-phase RPA on the nanoplasmonic microarray functions effectively, even when applied to clinical nasopharyngeal swab samples.

We compared our nanoplasmonic microarray–based solid-phase RPA method with multiplex platforms such as Luminex xTAG, BioFire FilmArray, and DNA microarray, as well as with previously reported solid-phase RPA methods and plasmonic-based nucleic acid detection methods, as shown in Table 3. Our assay method demonstrates superior sensitivity and stands out in terms of multiplex capability and analysis time compared to other methods. Our assay facilitates high-multiplex analysis by simply increasing the number of immobilized forward primers. However,

Table 3 Comparison with commercial multiplex assays, previously reported solid-phase RPA assays, and plasmonic-based nucleic acid detection methods

Methods Ref	Amplification method	Detection method	Analytical sensitivity	Multiplex capability	Detection time (post-pretreatment)
Luminex xTAG [3, 4]	PCR	Fluorescent-barcoded paramagnetic beads and flow cytometry	10^2 copies/μL (2×10^3 copies/rxn)	> 100	60 min
BioFire FilmArray [5, 6]	PCR	Fluorescence melting curve analysis	500 copies/mL (1.5×10^2 copies/rxn)	> 40	45–60 min
DNA microarray [13]	PCR	Fluorescence	10^3 copies/μL (1.5×10^4 copies/rxn)	High	> 150 min
[18]	Solid-phase RPA	Colorimetric detection	363 fM	No	50 min
[19]	Solid-phase RPA	Electrochemical detection	13 fM	Low	15 min
[17]	Solid-phase RPA	Electrochemical detection	0.1 fM	Low	60 min
[20]	Solid-phase RPA–coupled CRISPR	LED flashlight visual detection	20 copies/μL (10^3 copies/rxn)	No	40 min
[31]	Amplification-free CRISPR/Cas12a	Surface-enhanced Raman spectroscopy	1 fM	No	30–40 min
[32]	Plasmonic digital PCR	Plasmonic-enhanced Fluorescence	10 copies/rxn	Low	25 min
[33]	RPA and Hybridization	Plasmonic-enhanced fluorescence	100 copies/rxn	High	2 h
Our assay	**Solid-phase RPA**	**Plasmonic-enhanced fluorescence**	**4 copies/rxn (16.7 zM)**	**High**	**35 min**

the colorimetric detection method using TMB or the visual detection method using LEDs faces challenges in applying high-multiplex analysis. Also, electrochemical detection requires the fabrication of complex electrode arrays, making it difficult to develop as a high-multiplex analysis platform. Furthermore, recently reported amplification-free CRISPR/Cas12a-SERS detection methods [31] and plasmonic digital PCR [32] have also limited multiplex capabilities. Although RPA and microarray hybridization on gold nanostructured film-PEF detection [33] has high multiplex capabilities, but require an additional hybridization process, resulting in a 2-h turnaround time.

In this study, we conducted RNA extraction and cDNA synthesis as part of the experimental procedure before performing solid-phase RPA. It is worth mentioning that recent advances have introduced techniques that enable amplification without the necessity of RNA extraction [34]. Furthermore, RPA itself allows for the direct addition of transcriptase to the reaction, eliminating the need for separate cDNA synthesis step. Our system requires one simple step of final washing, but simple automated pipetting system or microfluidic system can be utilized. Consequently, nanoplasmonic-based solid-phase multiplex RPA not only has potential to achieve high sensitivity and extensive multiplexing capabilities but also simplifies development of automation equipment. This applicability for high-throughput testing is particularly valuable in situations where widespread testing is essential.

Conclusion

In this study, we have demonstrated potential of nanoplasmonic microarrays combined with solid-phase amplification for highly sensitive and extensive multiplexed molecular diagnostics. We demonstrated their specificity and sensitivity (LOD of four copies/reaction) through multiplex detection for E, N, and RdRP genes of SARS-CoV-2. We tested clinical respiratory swab samples ($n=30$) consisting of SARS-CoV-2 wild type ($n=10$), Omicron mutation BA.1 ($n=5$), Omicron mutation BA.2 ($n=5$), and negative samples ($n=10$), resulting in 100% consistency with PCR results across all samples. This technology has ability to perform extensive multiplexing, allowing simultaneous detection of multiple targets in a single reaction, significantly improving diagnostic efficiency and throughput. Taken together, rapidity, high sensitivity, specificity, multiplexing capability, and ability to simplify equipment of this technology highlight its potential for broad applications in clinical diagnostics and public health surveillance.

Supplementary Information The online version contains supplementary material available at https://doi.org/10.1007/s00604-024-06723-4.

Author contributions Ji Young Lee conducted analytical experiments, developed the methodology, and wrote the main manuscript text.

Min-Young Lee conceived the idea, contributed to the methodology and wrote the main manuscript text.

Sung-Gyu Park fabricated the device.

Hyowon Jang performed analytical experiments.

Sunjoo Kim provided resources and contributed to the methodology.

Taejoon Kang provided resources and contributed to the methodology.

Funding This study was supported by the Technology Innovation Program (RS-2024-00432381 and RS-2024–00432382) funded by the Ministry of Trade, Industry & Energy(MOTIE, Korea), KRIBB Research Initiative Program (KGM5472413), and National R&D Program (NRF-2021M3H4A1A02051036) through National Research Foundation of Korea (NRF) funded by Ministry of Science and ICT.

Data Availability Data will be made available on request.

Declarations

Competing interests The authors declare no competing interests.

Open Access This article is licensed under a Creative Commons Attribution-NonCommercial-NoDerivatives 4.0 International License, which permits any non-commercial use, sharing, distribution and reproduction in any medium or format, as long as you give appropriate credit to the original author(s) and the source, provide a link to the Creative Commons licence, and indicate if you modified the licensed material. You do not have permission under this licence to share adapted material derived from this article or parts of it. The images or other third party material in this article are included in the article's Creative Commons licence, unless indicated otherwise in a credit line to the material. If material is not included in the article's Creative Commons licence and your intended use is not permitted by statutory regulation or exceeds the permitted use, you will need to obtain permission directly from the copyright holder. To view a copy of this licence, visit http://creativecommons.org/licenses/by-nc-nd/4.0/.

References

1. Kudo E, Israelow B, Vogels CBF, Lu P, Wyllie AL, Tokuyama M, Venkataraman A, Brackney DE, Ott IM, Petrone ME, Earnest R, Lapidus S, Muenker MC, Moore AJ, Casanovas-Massana A, Yale IMPACT Research Team, Omer SB, Dela Cruz CS, Farhadian SF, Ko AI, Grubaugh ND, Iwasaki A (2020) Detection of SARS-CoV-2 RNA by multiplex RT-qPCR. PLoS Biol 18(10):e3000867
2. Lam D, Luu PL, Song JZ, Qu W, Risbridger GP, Lawrence MG, Lu J, Trau M, Korbie D, Clark SJ, Pidsley R, Stirzaker C (2020) Comprehensive evaluation of targeted multiplex bisulphite PCR sequencing for validation of DNA methylation biomarker panels. Clin Epigenetics 12(1):90
3. Purohit S, Sharma A, She JX (2015) Luminex and other multiplex high throughput technologies for the identification of, and host response to, environmental triggers of type 1 diabetes. Biomed Res Int 2015:326918
4. Cong F, Zhu Y, Wang J, Lian Y, Liu X, Xiao L, Huang R, Zhang Y, Chen M, Guo P (2018) A multiplex xTAG assay for the simultaneous detection of five chicken immunosuppressive viruses. BMC Vet Res 14:347
5. Poritz MA, Blaschke AJ, Byington CL, Meyers L, Nilsson K, Jones DE, Thatcher SA, Robbins T, Lingenfelter B, Amiott E, Herbener A, Daly J, Dobrowolski SF, Teng DH, Ririe KM (2011) FilmArray, an automated nested multiplex PCR system for multipathogen detection: development and application to respiratory tract infection. PLoS One 6(10):e26047
6. Sanchez AO, Ochoa AR, Hall SL, Voelker CR, Mahoney RE, McDaniel JS, Blackburn A, Asin SN, Yuan TT (2022) Comparison of next generation diagnostic systems (NGDS) for the detection of SARS-CoV-2. J Clin Lab Anal 36:e24285
7. Chang LJ, Hsiao CJ, Chen B, Liu TY, Ding J, Hsu WT, Su-Ortiz V, Chen ST, Su KY, Wu HP, Lee CC (2021) Accuracy and comparison of two rapid multiplex PCR tests for gastroenteritis pathogens: a systematic review and meta-analysis. BMJ Open Gastroenterol 8(1):e000553
8. Chen H, Weng H, Lin M, He P, Li Y, Xie Q, Ke C, Jiao X (2017) The clinical significance of FilmArray respiratory panel in diagnosing community-acquired pneumonia. Biomed Res Int 2017:7320859
9. Bednár M (2000) DNA microarray technology and application. Med Sci Monit 6(4):796–800
10. Marzancola MG, Sedighi A, Li PC (2016) DNA microarray-based diagnostics. Methods Mol Biol 1368:161–178
11. Diaz E, Barisone GA (2011) DNA microarrays: sample quality control, array hybridization, and scanning. J Vis Exp 49:2546
12. Sartor M, Schwanekamp J, Halbleib D, Mohamed I, Karyala S, Medvedovic M, Tomlinson CR (2004) Microarray results improve significantly as hybridization approaches equilibrium. Biotechniques 36(5):790–796
13. Ma X, Li Y, Liang Y, Liu Y, Yu L, Li C, Liu Q, Chen L (2020) Development of a DNA microarray assay for rapid detection of fifteen bacterial pathogens in pneumonia. BMC Microbiol 20(1):177
14. Kersting S, Rausch V, Bier FF, von Nickisch-Rosenegk M (2014) Multiplex isothermal solid-phase recombinase polymerase amplification for the specific and fast DNA-based detection of three bacterial pathogens. Mikrochim Acta 181(13–14):1715–1723
15. Chin WH, Sun Y, Høgberg J, Hung TQ, Wolff A, Bang D (2017) Solid-phase PCR for rapid multiplex detection of Salmonella spp. at the subspecies level, with amplification efficiency comparable to conventional PCR. Anal Bioanal Chem 409(10):2715–2726
16. Kim J, Jung S, Byoun MS, Yoo C, Sim SJ, Lim CS, Kim SW, Kim SK (2018) Multiplex real-time PCR using temperature-sensitive primer-supplying hydrogel particles and its application for malaria species identification. PLoS One 13(1):e0190451
17. Ichzan AM, Hwang SH, Cho H, Fang CS, Park S, Kim G, Kim J, Nandhakumar P, Yu B, Jon S, Kim KS, Yang H (2021) Solid-phase recombinase polymerase amplification using an extremely low concentration of a solution primer for sensitive electrochemical detection of hepatitis B viral DNA. Biosens Bioelectron 179:113065
18. Jauset-Rubio M, Ortiz M, O'Sullivan CK (2021) Solid-phase primer elongation using biotinylated dNTPs for the detection of a single nucleotide polymorphism from a fingerprick blood sample. Anal Chem 93(44):14578–14585
19. Ortiz M, Jauset-Rubio M, Kodr D, Simonova A, Hocek M, O'Sullivan CK (2022) Solid-phase recombinase polymerase amplification using ferrocene-labelled dNTPs for electrochemical detection of single nucleotide polymorphisms. Biosens Bioelectron 198:113825
20. Qin X, Paul R, Zhou Y, Wu Y, Cheng X, Liu Y (2023) Multiplex solid-phase RPA coupled CRISPR-based visual detection of SARS-CoV-2. Biosens Bioelectron X 14:100381
21. Park S-G, Xiao X, Min J, Mun C, Jung HS, Giannini V, Weissleder R, Maier SA, Im H, Kim D-H (2019) Self-assembly of nanoparticle-spiked pillar arrays for plasmonic biosensing. Adv Funct Mater 29(43):1904257
22. Mercier JF, Slater GW, Mayer P (2003) Solid phase DNA amplification: a simple Monte Carlo lattice model. Biophys J 85(4):2075–2086

23. Woo A, Jung HS, Kim DH, Park SG, Lee MY (2021) Rapid and sensitive multiplex molecular diagnosis of respiratory pathogens using plasmonic isothermal RPA array chip. Biosens Bioelectron 182:113167
24. Piliarik M, Vaisocherova H, Homola J (2007) Towards parallelized surface plasmon resonance sensor platform for sensitive detection of oligonucleotides. Sens Actuators B Chem 121(1):187–193
25. Tao Z, Zhou Y, Li X, Wang Z (2020) Competitive HRP-linked colorimetric aptasensor for the detection of fumonisin B1 in food based on dual biotin-streptavidin interaction. Biosensors (Basel) 10(4):31
26. Mavrogiannopoulou E, Petrou PS, Koukouvinos G, Yannoukakos D, Siafaka-Kapadai A, Fornal K, Awsiuk K, Budkowski A, Kakabakos SE (2015) Improved DNA microarray detection sensitivity through immobilization of preformed in solution streptavidin/biotinylated oligonucleotide conjugates. Colloids Surf B Biointerfaces 128:464–472
27. Deng L, Kitova EN, Klassen JS (2013) Dissociation kinetics of the streptavidin-biotin interaction measured using direct electrospray ionization mass spectrometry analysis. J Am Soc Mass Spectrom 24(1):49–56
28. Gandra N, Portz C, Tian L, Tang R, Xu B, Achilefu S, Singamaneni S (2014) Probing distance-dependent plasmon-enhanced near-infrared fluorescence using polyelectrolyte multilayers as dielectric spacers. Angew Chem Int Ed Engl 53(3):866–870
29. Peters JP, Maher LJ (2010) DNA curvature and flexibility in vitro and in vivo. Q Rev Biophys 43(1):23–63
30. Zhang CY, Zhang NH (2022) Mechanical constraint effect on DNA persistence length. Molecules 27(22):7769
31. Liang J, Teng P, Xiao W, He G, Song Q, Zhang Y, Peng B, Li G, Hu L, Cao D, Tang Y (2021) Application of the amplification-free SERS-based CRISPR/Cas12a platform in the identification of SARS-CoV-2 from clinical samples. J Nanobiotechnology 19(1):273
32. Kim KH, Ryu E, Khaleel ZH, Seo SE, Kim L, Kim YH, Park HG, Kwon OS (2024) Plasmonic digital PCR for discriminative detection of SARS-CoV-2 variants. Biosens Bioelectron 246:115859
33. Liu Y, Yang Y, Wang G, Wang D, Shao PL, Tang J, He T, Zheng J, Hu R, Liu Y, Xu Z, Niu D, Lv J, Yang J, Xiao H, Wu S, He S, Tang Z, Liu Y, Tang M, Jiang X, Yuan J, Dai H, Zhang B (2023) Multiplexed discrimination of SARS-CoV-2 variants via plasmonic-enhanced fluorescence in a portable and automated device. Nat Biomed Eng 7(12):1636–1648
34. Wee SK, Sivalingam SP, Yap EPH (2020) Rapid direct nucleic acid amplification test without RNA extraction for SARS-CoV-2 using a portable PCR thermocycler. Genes 11(6):664

Publisher's Note Springer Nature remains neutral with regard to jurisdictional claims in published maps and institutional affiliations.